Experimental Aeroelastic Behavior of Unswept and Forward-Swept Cantilever Graphite/Epoxy Wings

Brian J. Landsberger*
6520 Test Group/Flight Simulator Branch, Edwards Air Force Base, California
and
John Dugundji†
Massachusetts Institute of Technology, Cambridge, Massachusetts

An analytical and experimental investigation was made of the aeroelastic deflections, divergence, and flutter behavior of both unswept and 30 deg forward-swept rectangular, graphite/epoxy, cantilevered plate-type wings, with various amounts of bending-torsion stiffness coupling. The analytical investigation used a Rayleigh-Ritz formulation together with incompressible three-dimensional Weissinger L-method aerodynamics for the divergence, and incompressible two-dimensional unsteady strip theory for the flutter. A semiempirical attempt was also made to obtain the steady airload deflections of the wing including the nonlinear stall behavior. Experiments on 13 wing configurations showed divergence and bending-torsion flutter at low angles of attack, and torsion and bending stall flutter at higher angles of attack. Good agreement with theory was found for the divergence and bending-torsion flutter cases at low angles of attack, and for the nonlinear steady wing deflections at high angles of attack. The +15° ply configuration was efficient in relieving the adverse divergence effect of the forward-swept wing.

Introduction

THE use of composite materials in aircraft structures has added another design dimension to the aircraft designer. These composite materials are useful not only for their high-strength-to-weight ratio, but also because they give the designer the ability to vary the force deflection behavior by varying the layup scheme, and, thus, have made some previously impractical design options attractive. In particular, forward-swept wings have gained renewed interest because their major drawback, low wing divergence speeds, can be significantly improved by using tailored composite material in wing construction. A good general discussion of this is given by Hertz et al.[1] Other detailed studies of forward-swept wings are given in Refs. 2-8. The later studies begin to explore the effects of rigid-body pitch modes on these forward-swept wings, which can introduce a low-frequency body freedom flutter to the problem.

The present paper is a continuation of previous work by Hollowell and Dugundji,[9] who explored the divergence and flutter behavior of a series of stiffness-coupled, graphite/epoxy, unswept cantilever plate wings. Using that work as a foundation, the present paper extends the range by investigating some new ply layup patterns and by investigating the 30 deg forward-sweep case as well. As before, both the low-angle-of-attack (linear) and high-angle-of-attack (nonlinear) aeroelastic properties of cantilever wings are explored. All static deflection, divergence, and flutter data are carefully documented and, as such, extend the experimental base for aeroelastic tailoring with composites. More extensive details of the analysis and experiment can be found in Ref. 10.

Received May 9, 1984; presented as Paper 84-0903 at the AIAA/ASME/ASCE/AHS 25th Structures, Structural Dynamics and Materials Conference, Palm Springs, Calif., May 14-16, 1984; revision received April 19, 1985. This paper is declared a work of the U.S. Government and therefore is in the public domain.

*Major, U.S. Air Force, Simulation Engineer.

†Professor, Department of Aeronautics and Astronautics. Member AIAA.

Analysis

The wings used in the experiments and modeled in the analysis were cantilevered flat graphite/epoxy laminate plates. For all tests, the flat-plate wings were mounted vertically in the wind tunnel. The corresponding swept-wing geometry is shown in Fig. 1, with a right-hand Cartesian axis system (z axis pointing into the paper along with positive deflection w, and positive lift L). The positive fiber ply direction θ_F for this investigation is also shown. All static and dynamic analyses were done using the Rayleigh-Ritz method with five modes to describe the lateral deflection w, namely,

$$w = \sum_{i=1}^{5} \gamma_i(\bar{x},\bar{y}) q_i(t) \tag{1}$$

where

$$\gamma_i = \phi_i(\bar{x})\psi_i(\bar{y}) \tag{2}$$

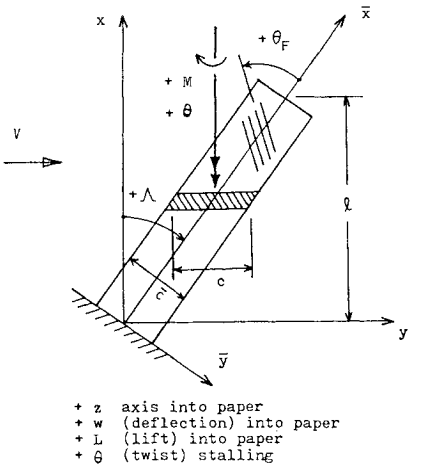

Fig. 1 Swept-wing coordinate system.

and $\phi_i(\bar{x})$ and $\psi_i(\bar{y})$ are nondimensional modes in the $\bar{x}$ and $\bar{y}$ directions, respectively, given by

$$\begin{aligned}
&\phi_1(\bar{x}) = \text{1st cantilever beam mode} && \psi_1(\bar{y}) = 1\\
&\phi_2(\bar{x}) = \text{2nd cantilever beam mode} && \psi_2(\bar{y}) = 1\\
&\phi_3(\bar{x}) = \sin(\pi\bar{x}/2\bar{\ell}) && \psi_3(\bar{y}) = \bar{y}/\bar{c}\\
&\phi_4(\bar{x}) = \sin(3\pi\bar{x}/2\bar{\ell}) && \psi_4(\bar{y}) = \bar{y}/\bar{c}\\
&\phi_5(\bar{x}) = \bar{x}/\bar{\ell}(1-\bar{x}/\bar{\ell}) && \psi_5(\bar{y}) = [4(\bar{y}/\bar{c})^2 - 1/3]
\end{aligned} \tag{3}$$

These modes represent first bending (1B), second bending (2B), first torsion (1T), second torsion (2T), and first chordwise bending (1C), respectively, and are the same modes used in the previous analysis by Hollowell and Dugundji.[9]

The strain energy U for a symmetric anisotropic laminate plate is[11]

$$\begin{aligned}
U = \frac{1}{2}\int_0^{\bar{\ell}} \int_{-\bar{c}/2}^{\bar{c}/2} [&D_{11}(w_{,\bar{x}\bar{x}})^2 + 2D_{12}w_{,\bar{x}\bar{x}}w_{,\bar{y}\bar{y}}\\
&+ D_{22}(w_{,\bar{y}\bar{y}})^2 + 4D_{16}w_{,\bar{x}\bar{x}}w_{,\bar{x}\bar{y}} + 4D_{26}w_{,\bar{y}\bar{y}}w_{,\bar{x}\bar{y}}\\
&+ 4D_{66}(w_{,\bar{x}\bar{y}})^2]\,\mathrm{d}\bar{y}\mathrm{d}\bar{x}
\end{aligned} \tag{4}$$

where a comma denotes partial differentiation, and the D_{ij}'s are the appropriate bending stiffnesses that depend on the fiber orientation and stacking sequence of the individual laminas. The kinetic energy T for the plate is

$$T = \frac{1}{2}\int_0^{\bar{\ell}} \int_{-\bar{c}/2}^{\bar{c}/2} m\dot{w}^2\,\mathrm{d}\bar{y}\mathrm{d}\bar{x} \tag{5}$$

where $(\dot{}) = \mathrm{d}/\mathrm{d}t$, $m = \rho_G t_G$ is the mass per unit area, ρ_G the density of graphite/epoxy, and t_G the total plate thickness. The change in external work δW_e can be expressed as

$$\delta W_e = \int_0^{\ell} \int_{-c/2}^{c/2} \Delta p_z \delta w\,\mathrm{d}y\mathrm{d}x \tag{6}$$

where Δp_z is the distributed lateral load per unit area. Finally, placing all of the previous terms into Lagrange equations results in the five equations of motion,

$$[M]\ddot{q} + [K]q = Q \tag{7}$$

where $[K]$ and $[M]$ are the appropriate stiffness and mass matrices resulting from strain and kinetic energies, while Q is the generalized force whose elements are given by

$$Q_i = \iint \gamma_i \Delta p_z \mathrm{d}x\mathrm{d}y \tag{8}$$

The elements of the $[K]$ and $[M]$ matrices are given in Refs. 9 (earlier version) and 10.

The structural deflection and twist behavior of the wing tip for a given applied tip load P can be obtained from Eq. (7) by neglecting the inertia terms $[M]\ddot{q}$ and setting the generalized forces $Q_1 = P\gamma_1(\bar{\ell})$, $Q_2 = P\gamma_2(\bar{\ell})$, and $Q_3 = Q_4 = Q_5 = 0$. Solving Eq. (7) for q and placing into Eq. (1) gives the desired deflections and twists. Similarly, the deflection behavior due to an applied tip twisting moment M_t can be obtained by setting $Q_1 = Q_2 = Q_5 = 0$, $Q_3 = -M_t/\bar{c}$, and $Q_4 = M_t/\bar{c}$ in Eq. (7).

Steady Airload Deflections and Divergence

The steady deflections of a wing in an airstream are obtained by combining the structural deflection characteristics of the wing together with the aerodynamic loads developed on the wing. Conventional linear theory for the structure and the aerodynamics will be assumed here. Later, the effects of aerodynamic nonlinearity will be examined.

The swept-wing geometry is shown in Fig. 1, with the z axis pointing into the paper, along with positive deflection w and positive lift L. The angle of attack θ of a wing section parallel to the oncoming flow, due to the elastic deformation of the wing $w(x,y)$, can be expressed as

$$\theta = -\frac{\partial w}{\partial y} = -\frac{\partial w}{\partial \bar{y}}\cos\Lambda - \frac{\partial w}{\partial \bar{x}}\sin\Lambda \tag{9}$$

Placing the assumed deflection pattern [Eq. (1)] into Eq. (9), one can express the elastic angle of attack θ at a number of spanwise stations x_i in matrix form as

$$\theta = [S]q \tag{10}$$

where

$$S_{ij} = -\frac{\partial \gamma_j}{\partial \bar{y}}(\bar{x}_i, \bar{y}_i)\cos\Lambda - \frac{\partial \gamma_j}{\partial \bar{x}}(\bar{x}_i, \bar{y}_i)\sin\Lambda$$

and the elements S_{ij} are evaluated at the three-quarter chord of each spanwise section. The total angle of attack α of each section is $\alpha = \alpha_0 + \theta$, where α_0 represents the root angle of attack of the wing.

The aerodynamic lift on each section of the wing is expressed as $L = q\,cC_\ell\Delta x$, where q is the dynamic pressure, c the chord, C_ℓ the local lift coefficient, and Δx the width of the section. To relate the lift to the local angle of attack, 3-dimensional Weissinger L-method theory for a finite swept wing in incompressible flow is used. This is presented by De Young and Harper[12] as

$$\alpha_i = \sum_{j=1}^{4} \frac{a_{ij}}{4\ell}(cC_\ell)_j \tag{11}$$

where ℓ is the semispan (see Fig. 1) and a_{ij} are nondimensional coefficients tabulated in Ref. 12 for different configurations at the Multhopp stations $x/\ell = 0.924$, 0.707, 0.383, and 0. In matrix form,

$$L = q[\bar{W}]cC_\ell \tag{12}$$

$$\alpha = [A]cC_\ell \tag{13}$$

where $[\bar{W}]$ is an appropriate section width diagonal matrix weighted for the Multhopp station distribution. Inverting Eq. (13) and placing into Eq. (12) gives the lift distribution L for a given angle-of-attack distribution α. The corresponding generalized force matrix Q is obtained by considering the lift loads as point loads acting at the one-quarter chord of the wing. Using Eq. (8), this gives

$$Q = [R]L \tag{14}$$

where the elements $R_{ij} = \gamma_i(\bar{x}_j, \bar{y}_j)$ are evaluated at the one-quarter chord of each section.

The steady airload deflections of the wing in an airstream are obtained by neglecting the inertia terms $[M]\ddot{q}$ in Eq. (7) and combining Eqs. (10-14) to give

$$\{(1/q)[I] - [D]\}\theta = [D]I\alpha_0 \tag{15}$$

where

$$[D] \equiv [S][K]^{-1}[R][\bar{W}][A]^{-1}$$

In the above, $[I]$ is a square unity matrix, I is a column of 1's, and α_0 the root angle of attack. Solution of Eq. (15) gives the elastic twist distribution θ, which is then added to α_0 to give the total α. The total lift loads L corresponding to this α is found from Eq. (12) and the inverted Eq. (13). Divergence for this linear problem occurs when the determinant of the left-hand side of Eq. (15) equals zero. This gives rise to the stan-

dard real eigenvalue problem,

$$[D]\theta = (1/q)\theta \tag{16}$$

The largest positive eigenvalue $1/q$ gives the lowest value of q for divergence. For some configurations, all of the eigenvalues are negative, thereby indicating no divergence possible for the wing.

The preceding steady airload and divergence analysis procedure was convenient for introducing 3-dimensional finite swept-wing aerodynamics into the modal analysis.

Flutter Analysis

The flutter analysis was done using the familiar V-g method.[13] A structural damping coefficient g is introduced into the equations of motion (7) to represent the amount of damping that must be added to the structure to attain neutral stability (flutter) at the given velocity. Assuming harmonic motion $q = qe^{i\omega t}$, the equations of motion (7) become

$$([K](1+ig) - \omega^2[M])qe^{i\omega t} = Q \tag{17}$$

where the generalized force Q, defined by Eq. (8), comes from the aerodynamic loadings. For the aerodynamics, 2-dimensional, incompressible, unsteady strip theory was used with sections taken parallel to the flow, as shown in Fig. 1. The change in external work δW_e of Eq. (6) is

$$\delta W_e = \int_0^{\ell} (L\delta h + M\delta\theta + N\delta\zeta)\mathrm{d}x = \sum_{i=1}^{5} Q_i \delta q_i \tag{18}$$

where the section forces and deflections here are taken at the midchord, and all twists θ and moments M are taken about an axis parallel to the x axis. The section forces and moments are defined as

$$L = \int \Delta p \mathrm{d}y$$

$$M = -\int (y - y_c)\Delta p \mathrm{d}y$$

$$N = \int \psi_5 \Delta p \mathrm{d}y \tag{19}$$

while the section deflection, twist, and camber changes are expressed from Eqs. (1-3) and (9) as

$$h = \phi_1 q_1 + \phi_2 q_2$$

$$\theta = -\frac{1}{\bar{c}}(\phi_3 q_3 + \phi_4 q_4)\cos\Lambda - \left(\frac{\mathrm{d}\phi_1}{\mathrm{d}\bar{x}} q_1 + \frac{\mathrm{d}\phi_2}{\mathrm{d}\bar{x}} q_2\right)\sin\Lambda$$

$$\zeta = \phi_5 q_5 \tag{20}$$

Using 2-dimensional, incompressible unsteady aerodynamic theory and including camber effects as adapted from Spielberg[14] and described in Ref. 9, the aerodynamic forces can be written as

$$L = \pi\rho\omega^2 b^3 \cos\Lambda \left(L_A \frac{h}{b} + L_B\theta + L_C \frac{\zeta}{b}\right) e^{i\omega t}$$

$$M = \pi\rho\omega^2 b^4 \cos\Lambda \left(M_A \frac{h}{b} + M_B\theta + M_C \frac{\zeta}{b}\right) e^{i\omega t}$$

$$N = \pi\rho\omega^2 b^3 \cos\Lambda \left(N_A \frac{h}{b} + N_B\theta + N_C \frac{\zeta}{b}\right) e^{i\omega t} \tag{21}$$

where $b = c/2$ represents the semichord, ρ is the air density, and the $\cos\Lambda$ factor accounts for the sweep. Combining Eqs. (18-21) gives the generalized force matrix Q in the form

$$Q = \pi\rho\omega^2 b^3 [A] q e^{i\omega t} \tag{22}$$

where the elements A_{ij} of the 5×5 aerodynamic matrix $[A]$ are complex functions of reduced frequency, $k = \omega b/V$. Expressions for A_{ij} are given by Landsberger.[10]

Combining the aerodynamic forces [Eq. (22)] with the structural representation [Eq. (17)] gives rise to the complex eigenvalue problem

$$[B]q = Z[K]q \tag{23}$$

where

$$[B] \equiv [M] + \pi\rho b^3 [A], \qquad Z \equiv (1+ig)/\omega^2$$

For given values of reduced frequency, $k = \omega b/B$ the complex coefficients A_{ij} are evaluated, and Eq. (23) is solved for the five complex eigenvalues Z. From these eigenvalues and from k, the ω, g, and V are determined. Plots of g and ω vs V characterize the flutter stability and frequencies of the wing. The ω values at $V \approx 0$ represent the natural frequencies with air-mass effects present. The natural frequencies in a vacuum are also determined from Eq. (23) by using a small value of air density ρ.

Nonlinear Steady Airload Deflections

Because the flat-plate wings were flexible and could deflect to large bending and twisting angles without failure, the wings would stall when the linear calculated divergence speed was approached or even exceeded. Accordingly, an attempt was made to calculate the nonlinear steady airload deflections and twist behavior using semiempirical approximations to the nonlinear lift and drag characteristics. On the other hand, the structural stiffness was found by static tests to remain within a few percent of linear even for large deflections, and, hence, a linear structural model was used. Only the analysis for the unswept wing case, $\Lambda = 0$ deg, was attempted.

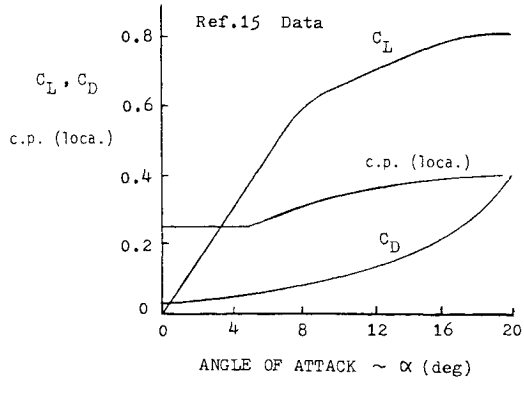

Fig. 2 Lift and drag coefficients for flat plate.

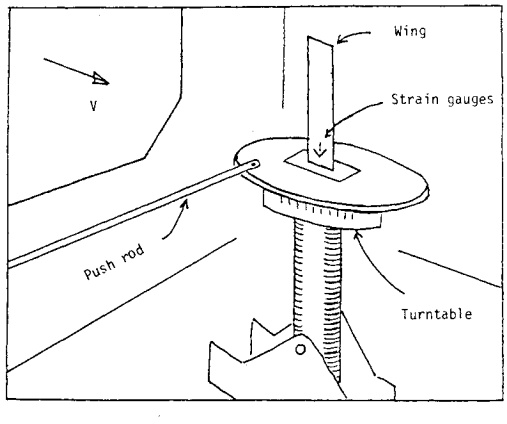

Fig. 3 Test setup in wind tunnel.

Figure 2 shows the measured lift and drag coefficients on a flat-plate wing as given by Riegels.[15] Also, an aft center-of-pressure movement was noticed from about 25% c at $\alpha = 5$ deg to 40% c at 20 deg. These force coefficient data were first resolved resolved in the direction normal to the chord, and then fitted by a simple power series in α. Then the pressure was distributed over the surface in the chordwise direction in a manner roughly resembling linear theory, but including the aft center-of-pressure movement. Finally, a spanwise tip correction was added to ensure the pressures fall to zero at the tips. The resulting approximation used for the pressure coefficient c_p is given below:

$$c_p = (-37.7\alpha^4 + 42.5\alpha^3 - 23.2\alpha^2 + 6.67\alpha) \times 1.11[1-(x/\ell)^9]\{(3.5-5.71\alpha)[0.5-(y/c)]^{2.5} \times 1.63\alpha\} + 3.5\alpha^3 \quad (24)$$

For further details and motivations, see Ref. 10. The angle of attack α to be used in the above can be approximated as

$$\alpha(x) = \alpha_0 - \frac{q_3}{c}\sin\frac{\pi x}{2\ell} \quad (25)$$

since the vast majority of the twist θ is from the first torsion mode, Eqs. (1) and (9).

To obtain a solution for the steady deflections and twist, a numerical iteration process is used. The rigid angle of attack α_0 is placed in Eq. (24) and the pressure coefficient c_p is evaluated at a number of chordwise and spanwise points on the wing. The pressures, $\Delta p_z = qc_p$, are then placed into Eq. (8) to obtain the generalized forces Q_i by numerical integration of the pressure distribution. Placing the Q_i into Eq. (7) without the mass term $[M]\ddot{q}$ allows one to solve for the deflections q. Placing this q into the static equation (25) gives a new $\alpha(x)$ distribution to start the process over again. For low airspeeds, three iterations were sufficient for convergence. At the higher speeds of this investigation, up to seven iterations were used.

Experiment

Experimental aeroelastic tests were conducted on a series of 13 flat-plate wings with different ply configurations at 0 and 30 deg forward sweep. The 0 deg sweep configurations complemented some earlier studies by Hollowell and Dugundji,[9] while the 30 deg forward-sweep configurations ($\Lambda = -30$ deg) were new.

The wing models for the tests were identical to those used in Ref. 9, and the properties are described more fully therein. Basically, each model had an effective length of 305 mm (12 in.) and a chord of 76 mm (3 in.), giving the wings a length-to-chord ratio $\ell/c = 4$. The models were all made up of 6 plies of Hercules AS1/3501-6 graphite/epoxy with 7 different ply layups, namely, $[0_2/90]_s$, $[+15_2/0]_s$, $[\pm 15/0]_s$, $[+30_2/0]_s$, $[\pm 30/0]_s$, $[+45_2/0]_s$, and $[\pm 45/0]_s$. By reversing the direction of flow, another 6 configurations were obtained, $[-15_2/0]_s$, $[\mp 15/0]_s$,..., to give a total of 13 configurations. These spanned a wide range of bending-torsion stiffness coupling ratio $D_{16}/\sqrt{D_{11}D_{66}}$ from -0.77 to $+0.77$ approximately.

Structural deflection tests were conducted on the wings by placing then in a stiff jig frame and subjecting them to force and moment couples applied near the tip, and carefully monitoring the resulting tip deflection and twist.

All wind tunnel tests were performed in the MIT Acoustic Wind Tunnel. This tunnel has continuous flow with a 1.5×2.3 m (5×7.5 ft) free-jet test section 2.3 m (7.5 ft) long located inside a large anechoic chamber, and can be varied continuously up to approximately 30 m/s (98.4 ft/s). The model was mounted vertically on a turntable which could readily be rotated to change the angle of attack. See Fig. 3. In addition, a large, heavy, swivel clamp joint at the wing root could be rotated to change the angle of sweep. For the present tests, only the unswept ($\Lambda = 0$ deg) and forward-swept ($\Lambda = -30$ deg) positions were investigated.

The wind tunnel tests were carefully monitored by video movies, photographs, and strain-gage strip charts in an attempt to obtain the static deflections and angles under airloads as well as the flutter-vibration amplitudes and frequencies. An overhead mirror was mounted above the test wings, and by proper angles, one could look down upon the wing tip and view it against a grid painted on the turntable base. Subsequent analysis of video movies taken under floodlight and strobe light conditions (to slow the motion), allowed one to

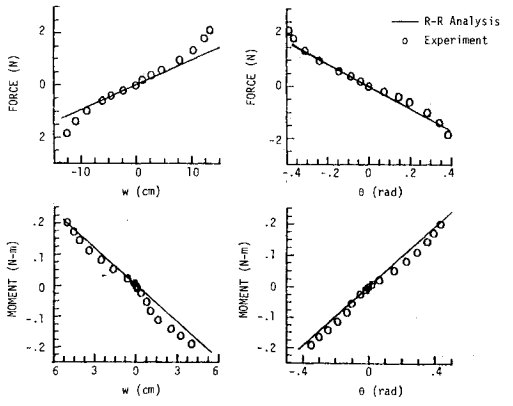

Fig. 4 Structural deflections of $[+30_2/0]_s$ wing.

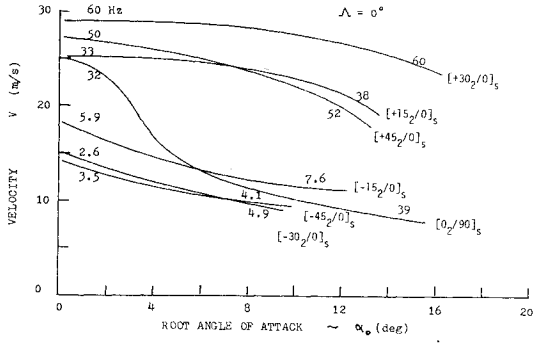

Fig. 5 Experimental flutter and divergence boundaries ($\Lambda = 0$ deg).

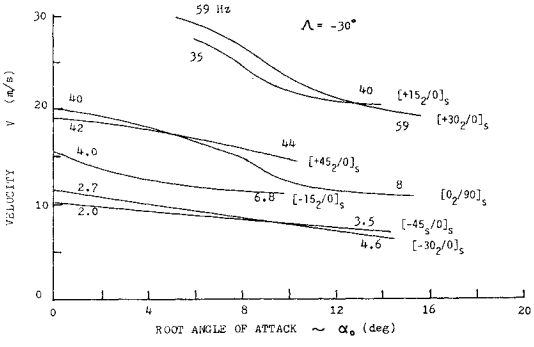

Fig. 6 Experimental flutter and divergence boundaries ($\Lambda = -30$ deg).

Table 1 Natural frequencies of wings

Wing	First bending		First torsion		Second bending	
	Theory, Hz	Experiment, Hz	Theory, Hz	Experiment, Hz	Theory, Hz	Experiment, Hz
$[0_2/90]_s$	10.8	10.5	39	44	67	—
$[+15_2/0]_s$	8.5	9.2	48	48	58	66
$[\pm 15/0]_s$	9.9	10.0	50	52	63	77
$[+30_2/0]_s$	6.0	7.1	60	60	41	44
$[\pm 30/0]_s$	7.8	8.0	65	68	50	—
$[+45_2/0]_s$	4.6	6.2	55	48	31	32
$[\pm 45/0]_s$	5.7	6.0	69	76	37	36

Table 2 Flutter data, unswept wings ($\Lambda = 0$ deg)

Wing	V, m/s	α_0, deg	w_{ave}, cm	Δw, cm	θ_{ave}, deg	$\Delta\theta$, deg	ω, Hz
$[0_2/90]_s$	26	1	0.5	0.7	1.0	10.3	33.0
	13	10	2.4	0	3.5	9.8	40.0
$[+15_2/0]_s$	25	1	0.2	0.2	0.7	8.1	32.0
	24	10	5.1	0.2	−4.0	19.3	37.0
$[\pm 15/0]_s$	28	3	4.0	0.8	−0.7	8.5	37.0
	16	10	3.8	0	0.4	5.0	49.0
$[\mp 15/0]_s$	21	1	4.3	0.5	4.8	14.0	43.0
	10	10	2.2	0.1	2.8	7.0	43.0
$[-15_2/0]_s$	18	1	4.7	9.4	10.1	17.4	5.8
	13	10	3.3	11.7	7.9	28.4	7.6
$[+30_2/0]_s$	29	0	−0.6	1.7	2.4	12.0	60.0
	28	12	7.9	4.0	−4.8	35.0	61.0
$[\pm 30/0]_s$	27	10	11.7	1.2	−3.7	12.0	46.0
$[\mp 30/0]_s$	24	1	13.5	1.3	13.5	8.8	40.0
	15	10	8.4	0.2	5.6	6.7	52.0
$[-30_2/0]_s$	15	1	5.1	17.2	3.9	16.0	2.6
	8	10	3.0	4.5	4.9	5.8	4.9
$[+45_2/0]_s$	27	1	2.1	3.6	2.2	23.0	25.0
	23	10	9.9	2.7	−2.7	20.0	26.0
$[\pm 45/0]_s$	25	8	13.1	0.4	−2.4	3.2	44.0
	18	10	10.8	0.6	−4.2	6.8	49.0
$[\mp 45/0]_s$	22	1	16.0	0.9	9.0	1.5	40.0
	14	10	12.2	0.1	6.3	6.3	55.0
$[-45_2/0]_s$	14	1	10.9	12.0	10.0	14.0	3.5
	9	10	5.2	10.3	5.2	9.1	4.2

obtain tip deflections and twists under both steady airloads and during flutter. The movies were taken both looking down upon the wing and looking directly at the wing.

Before each wind tunnel test, the natural-vibration frequency of a wing was checked. With the wing mounted for the wind tunnel test, a simple initial deflection in twist and bending was given to the wing and then quickly released. The resulting oscillations picked up by the strain gages were recorded on a strip chart, and gave a good estimate of the bending and torsion frequencies of the wing.

For the wind tunnel tests, the wings were set at zero angle of attack and the tunnel was run up to a given airspeed. The angle of attack was then varied to check for possible flutter conditions. If flutter was found, the strain-gage signals were recorded and the frequency additionally checked with a strobe light. After finishing tests at that airspeed, the angle of attack was reduced, the airspeed increased by 1 m/s, and the test procedure was repeated. This allowed the flutter boundary curve of flutter speed vs root angle of attack to be mapped out for a wing. After the flutter boundary curve was defined, certain points were selected for further examination. For these tests, more complete records were taken, including video movies and photographs, to check the flutter amplitudes, frequencies, and average static positions of the wing. In addition, on the unswept wings ($\Lambda = 0$ deg), tests were run at several fixed airspeeds to observe the variation of steady wing tip deflection and twist with root angle of attack under steady airload conditions.

Results

The present studies explored the nonlinear as well as the linear aspects of flutter and divergence. The models were sufficiently flexible so that when they actually fluttered or diverged they were not destroyed, but rather went into steady-state limit cycles that were limited by the nonlinear airforces (stalling).

The structural deflection and twist characteristics of a typical wing under given applied forces and moments are given in Fig. 4, along with the analytical Rayleigh-Ritz predictions. Since the wings were 30.5 cm long, the deflections are over large ranges. The linear 5-mode Rayleigh-Ritz analysis gave good correlation for small amplitudes, including the bending-torsion stiffness coupling involving the twist θ due to force F and the deflection w due to moment M. For one case, the $[\pm 15/0]_s$ layup wing, a small snap buckling occurred due to slight camber imperfections resulting from ply layup fiber angle inaccuracies.

The natural frequencies of the wings are given in Table 1. These were found from the initial deflection tests prior to the wind tunnel runs, and agreed reasonably well with the theoretical calculations and with previous values given by Ref. 9 and Jensen et al.[16] Occasionally, the third mode could not be picked out by the transient decay.

The flutter and divergence characteristics of these wings are presented in Figs. 5 and 6 for the unswept and forward-swept wings, respectively. This data is experimental, and was taken in 1-deg increments of angle of attack. The curves shown were

drawn through the data points. These plots of flutter speed vs root angle of attack give the nonlinear (high-angle-of-attack) behavior as well as the linear (low-angle-of-attack) behavior. The frequency (Hz) of the resulting oscillations is also indicated on the graphs in order to show the change in flutter modes. As in Ref. 9, four different types of aeroelastic phenomena are observed; bending-torsion flutter ($\omega_h < \omega < \omega_\alpha$) and divergence at low tip angles of attack, and torsion stall flutter ($\omega \approx \omega_\alpha$) and bending stall flutter ($\omega \approx \omega_h$) at high tip angles of attack. The sharp drop in torsion stall flutter speed vs root angle of attack was also reported by Rainey[17] for thin, solid aluminum (isotropic) wings, and probably results from the tip section statically twisting to the neighborhood of the stall angle and then going in and out of stall. Further studies of torsion stall flutter were also conducted by Dugundji and Aravamudan[18] and Dugundji and Chopra[19] on 2-dimensional sections. The bending stall flutter is not very familiar, and was reported earlier in Ref. 9. The divergence condition was noted when the angle of attack could not be set small enough to keep the wing from "flipping over" to either one side or the other. Generally, a bending stall oscillation at the low bending frequency would then begin for these flexible wings. In Figs. 5 and 6, the linear divergence condition at low root angles of attack α_0 is identified by the low frequency of oscillation in comparison to the much higher frequency of the bending-torsion flutter oscillations.

The amplitudes, frequencies, and average static positions of the resulting flutter oscillations for the different wings are shown in Tables 2 and 3. In these tables, V, α_0, and ω are the air velocity, root angle of attack, and flutter frequency, respectively, while $w_{ave} = (w_{max} + w_{min})/2$ is the average wing tip deflection, $\Delta w = w_{max} - w_{min}$ is the double amplitude of the tip deflection oscillations, $\theta_{ave} = (\theta_{max} + \theta_{min})/2$ is the average wing tip elastic twist, and $\Delta\theta = \theta_{max} - \theta_{min}$ is the double amplitude of the tip twist oscillations. For each wing, generally one low and one high root angle-of-attack condition is shown. All of these were measured visually from the video movies and photos, and give some interpretation of the nonlinear flutter behavior indicated in Figs. 5 and 6. In particular, the character of the flutter, whether of a bending or a torsional nature, and the associated frequency, are apparent.

The linear flutter and divergence characteristics of the wings at low root angles of attack are shown in Fig. 7 for the $[+\theta_2/0]_s$ family of wings. Similar, but less dramatic, results were obtained for the $[\pm\theta/0]_s$ family. Figure 7 represents a crossplot from the data of Figs. 5 and 6 at $\alpha_0 = 0$. For negative ply angles θ_F and forward-sweep ($\Lambda = -30$ deg), divergence

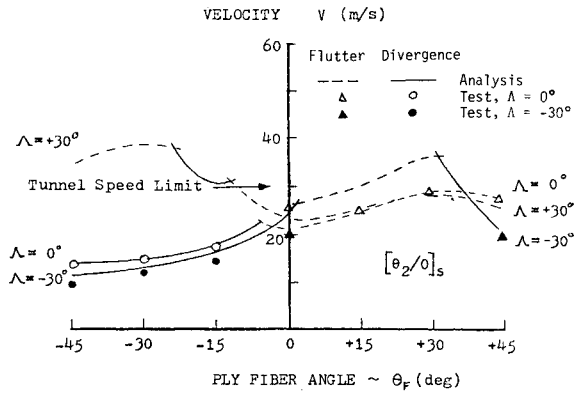

Fig. 7 Flutter and divergence at low angles α_0.

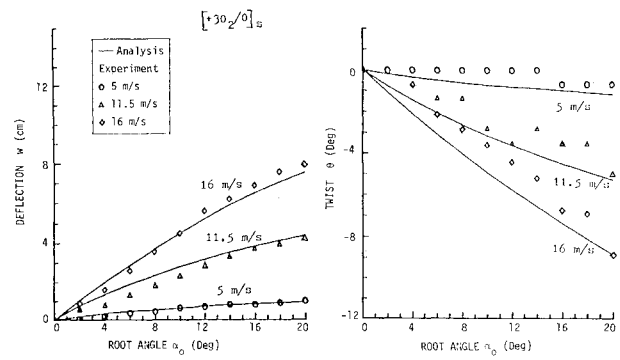

Fig. 8 Steady airload deflections of $[+30_2/0]_s$ wing.

Table 3 Flutter data, forward-swept wings ($\Lambda = -30$ deg)

Wing	V, m/s	α_0 deg	w_{ave}, cm	Δw, cm	θ_{ave}, deg	$\Delta\theta$, deg	ω, Hz
$[0_2/90]_s$	20	1	8.8	0	6.1	1.5	40.0
	18	10	8.3	11.0	1.5	3.0	8.0
$[+15_2/0]_s$	21	10	12.2	1.1	−10.7	16.7	40.0
$[\pm 15/0]_s$	25	1	7.8	0	−1.6	27.0	44.0
	18	10	8.0	0	−0.4	14.3	50.0
$[\mp 15/0]_s$	19	1	6.2	11.9	4.8	9.5	4.7
	15	10	5.2	12.8	4.7	9.3	7.5
$[-15_2/0]_s$	15	1	3.2	15.0	8.3	23.4	4.0
	12	10	3.9	12.9	7.7	18.1	6.8
$[+30_2/0]_s$	21	10	14.5	0.8	−18.0	12.0	59.0
$[\pm 30/0]_s$	22	1	19.8	0.7	−6.0	44.0	33.0
	20	10	21.5	1.0	−7.0	42.0	31.0
$[\mp 30/0]_s$	17	1	6.9	19.7	4.0	12.0	3.0
	13	10	7.5	9.5	2.5	5.0	5.6
$[-30_2/0]_s$	11	1	4.1	18.1	7.0	22.0	2.7
	8	10	3.7	10.9	3.5	17.0	4.6
$[+45_2/0]_s$	20	1	16.9	0.2	6.9	25.0	42.0
	15	10	16.9	0.7	14.5	19.1	44.0
$[\pm 45/0]_s$	20	1	19.5	3.0	−10.5	11.0	5.7
	14	10	12.9	6.3	3.5	21.0	4.8
$[\mp 45/0]_s$	14	2	9.5	19.0	5.5	11.0	2.8
	11	10	9.0	14.0	1.5	1.0	4.3
$[-45_2/0]_s$	10	1	7.1	8.6	8.4	14.7	2.0
	8	10	6.9	11.6	7.5	15.0	3.5

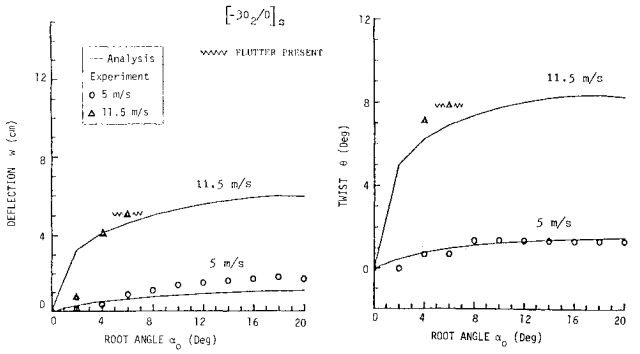

Fig. 9 Steady airload deflections of $[-30_2/0]_s$ wing.

dominates the aeroelastic behavior. Going to positive ply angles increases the divergence speed of the forward-swept wing, and a higher flutter speed now limits the flight speed. However, too much positive ply angle (+45°) results in a low divergence speed again since the bending stiffness becomes too low, and the bending-torsion stiffness coupling cannot overcome the geometric divergence tendency. A positive ply angle layup $[+15_2/0]_s$ seemed to be about optimum here, both from Fig. 7 and Figs. 5 and 6. The linear 5-mode flutter and divergence analyses gave good correlation with these experimental results, particularly for the divergence, where 3-dimension aerodynamic theory was used. It should be noted that the experimental and theoretical trends shown in Fig. 7 are also similar to the theoretical trends shown in Fig. 7 of Hertz et al.[1]

The nonlinear steady airload deflections and twists of the wing tip are shown in Figs. 8 and 9 for two contrasting wings, $[+30_2/0]_2$ and $[-30_2/0]_s$, with no sweep ($\Lambda = 0$ deg). These were obtained from visual inspection of the resulting video movies and photos of the test, and show a highly nonlinear relation with root angle of attack, particularly for the $[-30_2/0]_s$ wing which diverges at 15 m/s. The contrasting character of the two wings, where one twists negatively (nose down) to offset the root angle-of-attack change while the other twists positively (nose up) to bring the tip rapidly to the stall condition, is readily apparent. The analytical calculations using the semiempirical nonlinear theory including stall effects described earlier, give a reasonable correlation with experiment.

Conclusions

An analytical and experimental investigation was made of the aeroelastic deflection, divergence, and flutter behavior of unswept and 30 deg swept-forward graphite/epoxy cantilevered plate wings, with various amounts of bending-torsion stiffness coupling, in incompressible flow. The present work extends an earlier investigation by Hollowell and Dugundji[9] on unswept wings. Both the low-angle-of-attack (linear) and high-angle-of-attack (nonlinear) properties were explored. The investigation extends the experimental base for aeroelastic tailoring with composites.

Structural deflection tests on the 6 ply composite plate-type wings, revealed reasonable linear bending and twisting behavior up to large deflections. The deflections, twists, and bending-twist couplings were generally well predicted by Rayleigh-Ritz analysis.

The divergence and flutter investigation showed the large variation in aeroelastic properties possible by changes in ply layups. Four different types of aeroelastic phenomena were observed; bending-torsion flutter and divergence at low tip angles of attack (linear range), and torsion stall flutter and bending stall flutter at high tip angles of attack (nonlinear range).

The flutter and divergence characteristics at low angles of attack were well predicted by linear theory. A 5-mode Rayleigh-Ritz analysis gave good correlation with experiment for divergence using 3-dimensional aerodynamics, and gave reasonable correlation with experiment for flutter using 2-dimensional, velocity parallel, unsteady aerodynamics. The effects of ply orientation were well predicted. A positive ply angle layup $[+15_2/0]_s$ seemed to have efficient bending-torsion coupling to overcome the adverse geometric divergence effect of the 30 deg forward-swept wing.

The amplitudes, frequencies, and average static position of selected flutter points were measured and recorded. This helped identify the severity and character of the flutter modes encountered. The nonlinear flutter tests gave additional insight into the stall behavior of thin flexible wings, which had been pointed out earlier by Rainey,[17] by identifying the role of the tip section static angle of attack.

Nonlinear steady airload deflections and twists of the wing tips were obtained, and gave a good indication as to how the wings were behaving aeroelastically. Analytical calculations using a semiempirical nonlinear theory including stalling effects gave reasonable correlation with experiment.

Acknowledgments

The authors wish to acknowledge the assistance of Robert Dare in the experiments and data reduction. Also, they wish to acknowledge the support of the U.S. Air Force and the Air Force Office of Scientific Research under Grant AFOSR 82-0071, Dr. Anthony Amos, technical monitor.

References

[1]Hertz, T. J., Shirk, M. H., Ricketts, R. H., and Weisshaar, T. A., "On the Track of Practical Forward Swept Wings," *Astronautics and Aeronautics*, Vol. 20, Jan. 1982, pp. 40-53.

[2]Krone, N. J., "Divergence Elimination with Advanced Composites," AIAA Paper 75-1009, Aug. 1975.

[3]Sherrer, V. C., Hertz, T. J., and Shirk, M. H., "Wind Tunnel Demonstration of the Aeroelastic Tailoring Applied to Forward Swept Wings," *Journal of Aircraft*, Vol. 18, Nov. 1981, pp. 976-983.

[4]Blair, M. and Weisshaar, T., "Swept Composite Wing Aeroelastic Divergence Experiments," *Journal of Aircraft*, Vol. 19, Nov. 1982, pp. 1019-1024.

[5]Weisshaar, T. A., Zeiler, T. A., Hertz, T. J., and Shirk, M. H., "Flutter of Forward Swept Wings," *Proceedings of 23rd AIAA/ASME/ASCE/AHS Structures, Structural Dynamics and Materials Conference,* New Orleans, La., May 1982, Pt. 2, pp. 111-121.

[6]Miller, G. D., Wykes, J. H., and Brosnan, M. J., "Rigid Body-Structural Mode Coupling on a Forward Swept Wing Aircraft," *Journal of Aircraft*, Vol. 20, Aug. 1983, pp. 696-702.

[7]Weisshaar, T. A. and Foist, B. L., "Vibration and Flutter of Advanced Composite Lifting Surfaces," *Proceedings of 24th AIAA/ASME/ASCE/AHS Structures, Structural Dynamics and Materials Conference*, Lake Tahoe, Nev., May 1983, Pt. 2, pp. 498-508.

[8]Noll, T. E., Eastep, F. E., and Calico, R. A., "Active Suppression of Aeroelastic Instabilities on a Forward Swept Wing," *Journal of Aircraft*, Vol. 21, March 1984, pp. 202-208.

[9]Hollowell, S. J. and Dugundji, J., "Aeroelastic Flutter and Divergence of Stiffness Coupled, Graphite/Epoxy Cantilevered Plates," *Journal of Aircraft*, Vol. 21, Jan. 1984, pp. 69-76.

[10]Landsberger, B. J., "Aeroelastic Properties of Straight and Forward Swept Graphite/Epoxy Wings," M. S. Thesis, Department of Aeronautics and Astronautics, Massachusetts Institute of Technology, Cambridge, Mass., Feb. 1983.

[11]Ashton, J. E. and Whitney, J. M., *Theory of Laminated Plates*, Technomic Publishing Co., Stamford, Conn., 1970.

[12]DeYoung, J. and Harper, C. W., "Theoretical Symmetrical Span Loading at Subsonic Speeds," NACA Rept. 921, 1948.

[13]Bisplinghoff, R. L., Ashley, H., and Halfman, R. L., *Aeroelasticity*, Addison-Wesley Publishing Co., Reading, Mass., 1955.

[14]Spielberg, I. N., "The Two-Dimensional Incompressible Aerodynamic Coefficients for Oscillatory Changes in Airfoil Camber," *Journal of the Aeronautical Sciences*, Vol. 20, June 1953, pp. 432-434.

[15]Riegels, F. W., *Airfoil Sections*, Butterworths Publishing House, London, 1961.

[16]Jensen, D. W., Crawley, E. F., and Dugundji, J., "Vibrations of Cantilevered Graphite/Epoxy Plates with Bending-Torsion Coupling," *Journal of Reinforced Plastics and Composites*, Vol. 1, July 1982, pp. 254-269.

[17]Rainey, G. A., "Preliminary Study of Some Factors which Affect the Stall-Flutter Characteristics of Thin Wings," NACA TN-3622, March 1956.

[18]Dugundji, J. and Aravamudan, K., "Stall Flutter and Nonlinear Divergence of a Two-Dimensional Flat Plate Wing," MIT Aeroelastic and Structures Research Laboratory, ASL-TR-159-6; Air Force Office of Scientific Research, AFOSR TR 74-1734, July 1974.

[19]Dugundji, J. and Chopra, I., "Further Studies of Stall Flutter and Nonlinear Divergence of Two-Dimensional Wings," MIT Aeroelastic and Structures Research Laboratory, ASRL TR 180-1; NASA CR-144924, Aug. 1975.